JMEPEG
https://doi.org/10.1007/s11665-022-07049-z

1059-9495/$19.00

TECHNICAL ARTICLE

Rheology, Crystallinity, and Mechanical Investigation of Interlayer Adhesion Strength by Thermal Annealing of Polyetherimide (PEI/ULTEM 1010) Parts Produced by 3D Printing

Musa Yilmaz, Necip Fazil Yilmaz, and Mahmut Furkan Kalkan

Submitted: 14 February 2022 / Revised: 12 April 2022 / Accepted: 30 April 2022

Fused deposition modeling (FDM) is a 3D printing technology in which the melt extrusion method is used for the production of thermoplastic parts. 3D printed thermoplastic materials produced by this method suffer from a particularly significant problem, however, namely poor interfacial bond formation that results in weak mechanical performance. This work proposes a thermal process to enhance the strength of the interlayer adhesion of 3D printed PEI thermoplastic materials. The annealing process was determined as a suitable post-processing procedure and was the focus of this work. Annealing was carried out in an oven at temperatures of 220, 225, 230, and 235 °C; it was determined that annealing performed at 225 °C in particular was highly desirable in terms of enhancing interlayer adhesion strength. In this work, characterization (FTIR, XRD, and SEM) and mechanical (tensile, bending, and hardness) analyses of 3D printed PEI were performed to better understand the strength of interlayer adhesion and overcome a mechanical performance limitation of this material. According to the tensile, bending, and hardness test results, the greatest improvements were found as increase of 10, 5, and 12%, respectively.

Keywords 3D printing, annealing, crystallinity, interlayer tensile strength, PEI, rheology

1. Introduction

Additive manufacturing has a promising future in the aerospace, military, automobile, communications, and biomedical sectors for processing limited amounts of complex, customized components (Ref 1). Production of functional objects with additive manufacturing has many advantages over traditional production methods (Ref 2, 3) as a technology that facilitates the supply of spare parts to companies through its use in production and repair. Moreover, additive manufacturing methods are a technology in which each layer is formed to create the geometry determined by the associated 3D CAD model (Ref 4, 5). It is possible to manufacture complex parts with highly complex geometries without the use of any tools or fixtures and without waste material. The most common additive manufacturing methods can be specified as fused deposition modeling (FDM), selective laser sintering (SLS), selective laser melting (SLM), and digital light processing (DLP) (Ref 6, 7).

Musa Yilmaz and **Mahmut Furkan Kalkan**, Department of Mechanical Engineering, Engineering Faculty, Gaziantep University, 27310 Gaziantep, Turkey; and **Necip Fazil Yilmaz**, Department of Mechanical Engineering, Engineering Faculty, Gaziantep University, 27310 Gaziantep, Turkey; and Board of Trustees, Hasan Kalyoncu University, 27010 Gaziantep, Turkey. Contact e-mail: msyilmaz@gantep.edu.tr.

FDM is one of the common techniques among additive manufacturing methods for producing thermoplastic parts. Stratasys Inc. firstly released this technology commercially in 1991 (Ref 8, 9). The popularity of the use of FDM is rapidly increasing in daily life, and academic and industrial studies. This comes from the developing production method in which parts with geometries that cannot be produced by other methods or that would otherwise require a long time to produce can be manufactured in a straightforward manner (Ref 10, 11). This method allows the construction of functionally working parts as well as prototype production using biocompatible and strong materials (Ref 12–14).

Acrylonitrile butadiene styrene (ABS), polylactic acid (PLA), polycarbonate (PC), polyether ether ketone (PEEK), polyetherimide (PEI/ULTEM), etc., were generally used for 3D printer filament working with FDM techniques (Ref 15,16). PEI, known as ULTEM 1010, is high-temperature polymer and the strongest material in common use in FDM (Ref 17). This filament material is a transparent, amorphous, and biocompatible thermoplastic (Ref 18). However, only a limited number of FDM machines can use this filament because of its high-temperature melting (Ref 19, 20). In addition, although PEI has higher strength compared to other FDM filaments, it has lower strength compared to products made of the same material using the plastic injection method (Ref 21, 22). One of the most important reasons for this is that FDM products, when built, have inherently weak interfacial bonding (Ref 23). When 3D printed parts are utilized in constructions, reduced interfacial strength can result in certain problems (Ref 24). FDM product is a result of bonding the layers formed by extruding the filaments. This is because each layer does not bond completely to the other while being extruded (Ref 25). The interlayer

Published online: 14 June 2022

mechanical characteristics are determined by polymer diffusion bonding across the interface.

The mechanical properties of PEI material are highly influenced by production conditions, which also affect the crystallinity of the PEI. This crystallinity is one of the determining factors of the mechanical properties of PEI polymers, which can range from soft and elastic to rigid and high strength. Some additives to the composition of polymers can increase the mechanical properties depending on the extent to which they increase the crystallinity of the polymer (Ref 26). These additives may be used to regulate particular physical and mechanical properties by acting as nucleation agents to trigger crystallization (Ref 27). Therefore, annealing of printed parts is another technique that can be used to increase the ratio of crystallinity to non-crystallinity. The strength of annealed 3D printed components can be improved through increased crystallinity and enhanced interfacial bonding (Ref 28).

Annealing is a useful method for increasing the mechanical characteristics of 3D products in the direction of deposition (Ref 29). Annealing is a heat treatment procedure that alters the physical and, in some cases, chemical characteristics of a polymer product. The process consists of the steps of heating a polymer product to a specified temperature, maintaining it at this temperature, and then slowly cooling the product to room temperature. The heat treatment process has been used to increase the crystallinity of polymers and to release residual thermal stresses (Ref 30-32). The point to be considered when performing heat treatment on such parts is the glass transition temperature. Polymer materials, which are kept slightly above the glass transition temperature and cooled slowly, increase their mechanical properties by taking a more stable and crystalline structure.

There have been a number of studies about increasing the mechanical properties of 3D products in the literature. Sharma et al. (Ref 33) utilized different process parameters such as layer thickness, infill percentage, and printing speed on mechanical properties of parts made from ABS filament. They proved that as infill percentage increases, both the tensile and compression properties of the material improve. On the other hand, they found that as layer thickness increases, it has a direct proportional effect on tensile and reverse compression. Rajpurohit et al. (Ref 25) worked on mechanical properties, as the tensile strength of PLA printed parts depends on raster angle, layer thickness, and raster width. They found that raster angle is the major determinant of strength on test coupons. While a 0° raster angle was determined to give the maximum strength, a 90° raster angle was found to give the minimum. Another important parameter was determined to be raster width in this work. The researchers stated that increasing the width of the raster to 600 μm increases strength, but as this width increases further the strength decreases due to the formation of voids. These voids were thought to initiate cracking. Han et al. (Ref 34) used an infrared laser to heat the interface between layers during the printing of PEI with an FDM printer. They reported that with the use of this method, a stronger bond was formed between the layers and the strength of the printed parts was increased. Singh et al. (Ref 35) aimed to improve the mechanical properties of printed ABS specimens using a heat treatment process. The researchers investigated the effect on mechanical properties due to annealing temperature and holding time under heat. They observed that in thermoplastic materials produced using the FDM method, the heat treatment applied above the glass temperature reduced the gaps between the filaments. As a result of mechanical tests, they statistically determined that the applied temperature is a much more important parameter than the waiting time. The point to be considered when performing heat treatment on such parts is the glass transition temperature. Bhandari et al. (Ref 36) found the heat treatment process can heal the interlayer tensile strength of FDM printed parts.

Previous research has provided some insight into the influence of annealing on the mechanical characteristics of 3D printed thermoplastic materials. However, they generally focused on standard print materials such as ABS and PLA, which have low strengths. In current commercial applications, the strengths of these materials are limited. In order to increase the strength of 3D printed products, it is crucial to work on new materials and comprise them in FDM. Additionally, previous research did not take into account the effects of annealing on the adhesion strength of 3D printed PEI material. In this study, the effect of the annealing process on the bond structure between the layers of the 3D printed PEI material was investigated. The purpose of this research is to examine the effects of annealing on the interlayer adhesion characteristics of extrusion-based 3D printed PEI/ULTEM1010 polymers in detail. Annealing processes were completed at different heat treatment temperatures with constant holding times. Annealing temperatures were initiated above the glass transition temperature of the PEI material, after which the temperature was gradually increased. The characterization and mechanical testing of PEI printed parts were compared according to annealing temperature.

2. Materials and Methods

2.1 Material

Polyetherimide (PEI/ULTEM 1010) polymer, which is known as an essential engineering material due to its superior mechanical properties and outstanding thermal and chemical resistance, was used in this study (Ref 37). PEI is regarded as one of the strongest FDM thermoplastics, and it is known to be an amorphous polymer. Table 1 summarizes the working conditions for PEI.

2.2 Material Printing and Annealing Process

A Fortus 450mc 3D printer, which has a build size of 406 × 355 × 406 mm with a layer resolution of ± 127 μm, was used to manufacture the test specimens. This 3D printer works with the fused deposition method (FDM). This work was carried out in two stages. In the first step, nine cubic samples

Table 1 Working condition and properties of PEI filament (Ref 17, 38)

Density	1.27 g/cm^3
Molecular formula	$C_{37}H_{24}O_6N_2$
Glass transition temperature (T_g)	215 °C
Extrusion tip temperature	400 °C
Max. build platform temperature	190 °C
Layer thickness	330 μm
Infill density	100%
Raster angle	0°/90°

were fabricated to define the limit of annealing temperatures. The initial annealing temperature for PEI was chosen to be 220 °C. The main reason for choosing this temperature is related to the glass transition temperature of the polymer materials. Previous research has shown that the polymer's annealing temperature should be higher than its glass transition temperature in order to improve mechanical performance (Ref 39–43). Therefore, the annealing process was started at 220 °C, which is reasonably close to the glass transition temperature of PEI (215 °C). In the first stage of this study, in order to determine the annealing temperature ranges, all specimens were subjected to different temperatures ranging from 220 to 300 °C in 10 °C increments. The particular focus, however, was on temperatures ranging from 220 to 235 °C, which were examined in 5 °C increments, during the second stage. A MagmaTherm (MT-1200) oven was used for the annealing process. The specimens were placed in the oven on a flat steel plate and heated at the above temperatures for three hours. After holding the temperature, the specimens were brought out of the oven to room temperature and allowed to cool.

2.3 Characterization and Testing

The chemical structure of the specimens was examined by Fourier transform infrared (FTIR) spectroscopy using a Shimadzu IRTracer-100 spectrometer at room temperature. All specimens were scanned in the wavenumber region between 4000 and 400 cm^{-1} at a resolution of 4 cm^{-1}. X-ray diffraction (XRD) analysis of annealed and unannealed PEI specimens was obtained via a RIGAKU Miniflex 600 XRD system using Cu Kα radiation. Scattering angles of 2θ were recorded from 10° to 70° at a scan speed of 0.02°min^{-1}. A Zeiss Gemini 300 scanning electron microscope (SEM) was used to obtain micrographs of the fractured surfaces of the 3D printed PEI specimens. The fracture surfaces of all PEI samples were studied to discuss the fracture effect on fibers. The specimens were coated with a thin layer of palladium/gold prior to SEM analysis. A Shimadzu AGX universal testing device (50 kN load capacity) was used for the tensile test of the annealed and unannealed samples. Standard tension tests conducted in accordance with ASTM D638 (Ref 44) were carried out with a strain rate ($\dot{\varepsilon}$) of 5 mm/min. All tests were carried out under room conditions at constant temperature and humidity. Five identical samples were produced for each test condition. Test values were evaluated by averaging the results of five successive measurements. The bending tests for annealed and unannealed specimens were accomplished using a Shimadzu AGX universal testing device (50 kN load capacity). The procedure outlined in ASTM D790-17 (Ref 45) was followed during the testing. A symmetric three-point bending test on a span of 30 mm was performed at a speed of 1.56 mm/sec. All bending tests were performed by averaging five specimens. Hardness test experiments were accomplished using a portable BAREISS HPE II D-type shore hardness tester (Bareiss Heinrich Prüfgerätebau GmbH, Oberdischingen, Germany). Shore D hardness tests were carried out according to the ASTM D2240-15 (Ref 46) standard. Hardness readings were taken from fifteen different locations for each 10 mm thick sample, and their averages were calculated. There was a 6 mm distance between each tested region. Shore hardness tests were executed at room temperature.

3. Results and Discussion

3.1 FTIR Spectroscopy Results

FTIR spectroscopy was used in order to infer the chemical and molecular structure of PEI samples and changes to their structures due to the annealing process. The FTIR spectra recorded to find the annealing temperature range in the preliminary experiments are shown in Fig. 1. The unannealed PEI specimen contains features characteristic of imide group absorptions at 1234 cm^{-1} (aromatic ether C-O-C), 1355 and 743 cm^{-1} (C-N stretching and bending), and at 1780 and 1720 cm^{-1} (typical of imide carbonyl symmetric and asymmetric stretches) (Ref 47). These characteristic imide group absorptions are the same in samples annealed at up to 270 °C. However, at greater annealing temperatures, the PEI material started to show signs of chemical degradation. Aromatic ether (C-O-C), and the C-N stretching and bending modes typical of imide carbonyl asymmetric and symmetric vibrations were no longer seen via peaks at 400 and 1800 cm^{-1} (Fig. 1). Therefore, it can be said that chemical degradation occurs in the bonds between molecules of the PEI polymer annealed between 270 and 300 °C. Depending on the examinations made on the samples heat-treated in the first step, the temperature ranges where the distortion does not occur above the glass transition temperature was found. In addition, physical deterioration (such as profile distortion and color change) were observed in the PEI material after the annealing process at high temperatures (Fig. 1). As a result of the heat treatment performed during the first stage, it was determined that the profile and color of the PEI specimens had changed due to thermal effects (profile distortion) above a temperature of 235 °C. When the PEI material is annealed at 300 °C, the sample melts completely and, obviously, the form of the material changes dramatically.

It was stated in previous studies that the annealing temperature of the polymer should be above its glass transition temperature to increase the resultant mechanical performance (Ref 39–43). For these reasons, the lower and upper limits of the annealing temperature range were determined to be 220 and 235 °C, respectively. Heat treatments were carried out in the oven at temperatures of 220, 225, 230 and 235 °C. The FTIR spectra recorded for the PEI samples from the second step of the study are shown in Fig. 2. The aim of the first stage of the tests was to determine the limits of the annealing temperature.

PEI samples annealed at 220, 225, 230, and 235 °C exhibited typical IR patterns which are similar to unannealed PEI sample, illustrating that annealed PEI still maintains the basic structure of the PEI polymer. However, FTIR peaks of for PEI annealed at 235 °C were lower in intensity than both the unannealed sample and specimens annealed at 220, 225, and 230 °C. In the FTIR spectra of samples, all samples generally show prominent absorbance (characteristic imide group absorptions) at approximately 743, 1234, 1355, 1720, and 1780 cm^{-1} (Ref 47).

3.2 XRD Results

The XRD patterns (for the 2θ range of 5° to 70°) of unannealed and annealed PEI specimens are displayed in Fig. 3. The x-ray spectra of all 3D printed specimens show the completely amorphous structure of PEI where the curves are broadband without any significant or distinct peaks within the

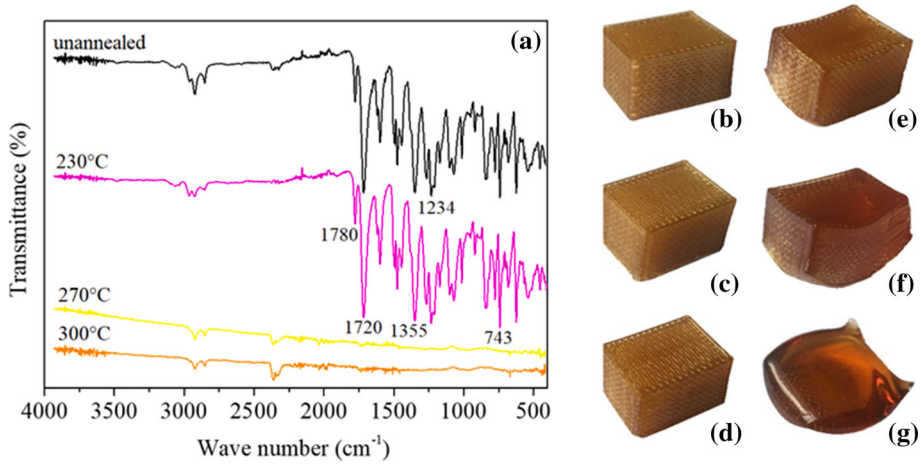

Fig. 1 (a) FTIR spectra of unannealed and annealed (at 230, 270, and 300 °C) PEI specimens, and the physical appearance of specimens when (b) unannealed, (c) annealed at 235 °C, (d) annealed at 240 °C, (e) annealed at 270 °C, (f) annealed at 280 °C, and g) annealed at 300 °C

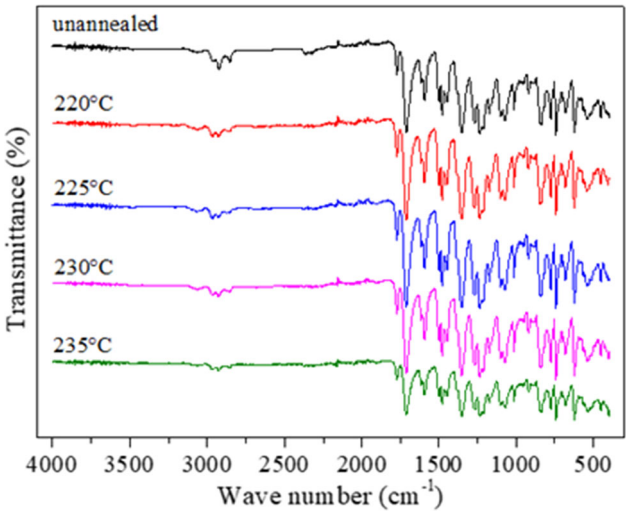

Fig. 2 FTIR spectra of unannealed and annealed (at 220, 225, 230 and 235 °C) PEI specimens

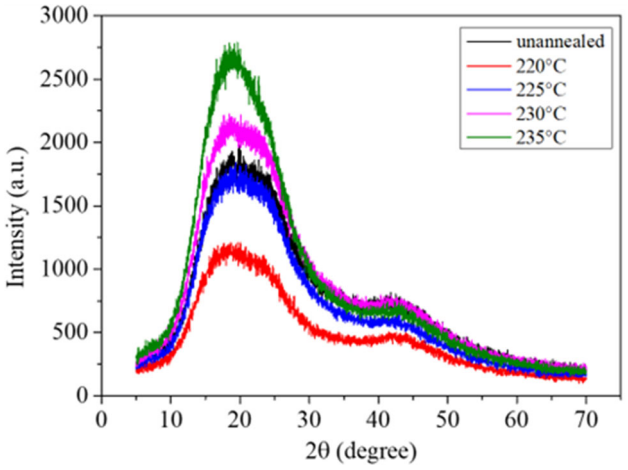

Fig. 3 XRD pattern of unannealed and annealed PEI specimens

scanned region. It was seen that XRD profiles have a broad peak centered at 2θ = 19.3° (Ref 48, 49), a weak peak at about 41.9°, and no detectable crystalline peaks. However, the intensity of the peak at 19.3° changed with the annealing operation applied to the PEI samples. As seen in the XRD graph, the annealed samples followed different trends to each other. Whereas samples annealed at 220 and 225 °C showed a lower measured intensity and hump than the unannealed sample, higher intensities and humps were observed in samples annealed at 230 and 235 °C. This indicates that the crystal forms and internal structures of PEI may have been altered according to the applied annealing operation (Ref 50).

3.3 Microstructural Analysis Results

The general microstructures and 3D printed structures of the PEI samples, including both transverse and longitudinal fibers' cross sections, are depicted in Fig. 4. The consecutive layers in the sample printed with a raster angle of 0°/90°, as shown in Fig. 4(a), are aligned with transverse fibers (0°) in the lower layer and longitudinal fibers (90°) in the upper layer, respectively. SEM microstructure views show the fracture surfaces after the tensile test. The SEM morphology of the tensile samples, consisting of two types of failure behavior, can be observed in Fig. 4(c), which are interfacial bond failure and fiber breakage. Since the tensile force acted on each of the fibers deposited in the longitudinal direction, almost all the fractures occurred at the fiber surfaces. However, if the tensile force acted on fiber deposited in the transverse direction, all of the fractures occurred at the interface.

The fracture surface of the longitudinal fibers (fiber breakage) was uniform and smooth, indicating that the breakage was a brittle fracture. However, as seen in Fig. 4(d), the interfacial bond failure region has two different forms of failure behavior: cohesive failure, and light-fiber-tear failure (Ref 51, 52). Light-fiber-tear failure is formed near the fiber surface at the interfacial bond region, and is characterized by the thin layer of the cavity. As the 3D printed product is weak in transverse tensile strength, peel stress generally dominates and starts the crack along the bondline in the interfacial bond region. Interfacial bond failure occurs when the adherend strength is the weakest, and depends on the strength of adhesion between two adjacent filaments.

The SEM micrograph recorded to examine the fracture surfaces formed after the tensile test is displayed in Fig. 5.

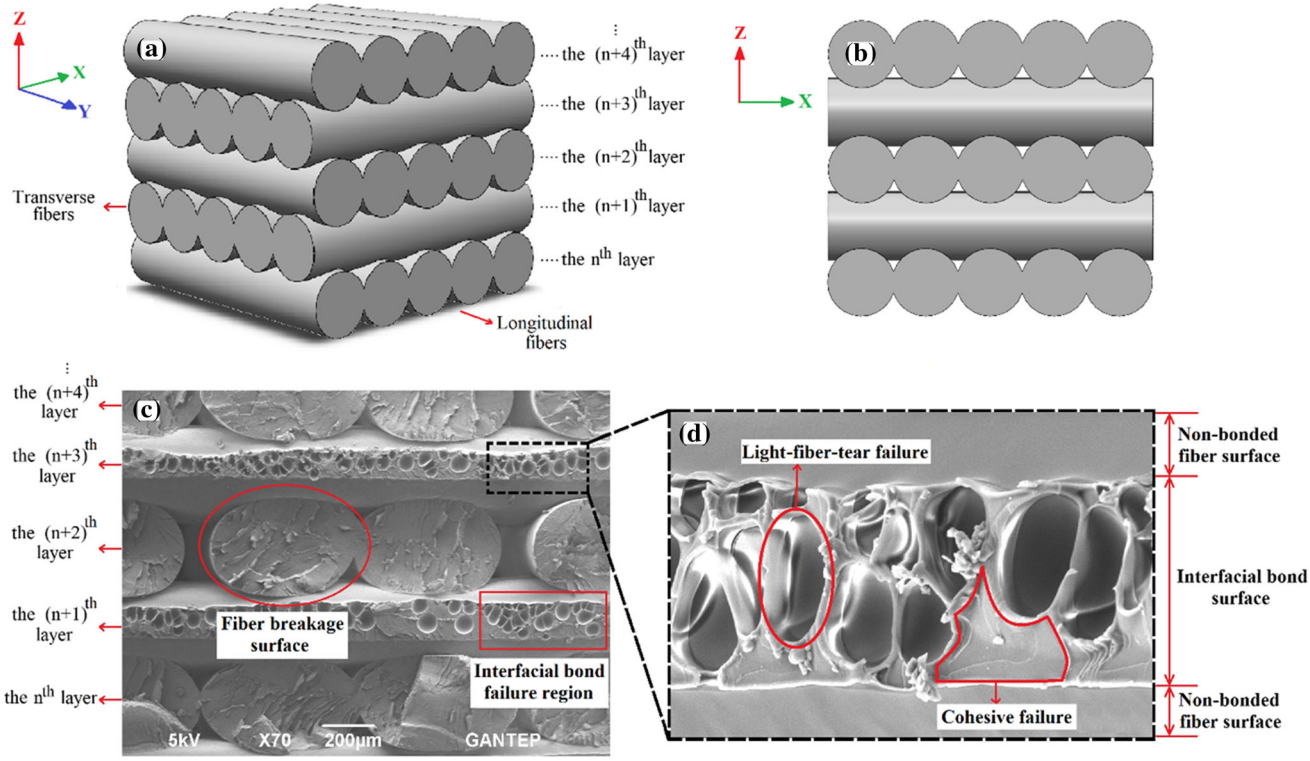

Fig. 4 3D printed structure of PEI specimen: (a) schematic illustration of perspective view, (b) schematic illustration of front view, (c) general SEM morphology, (d) general interfacial surface image

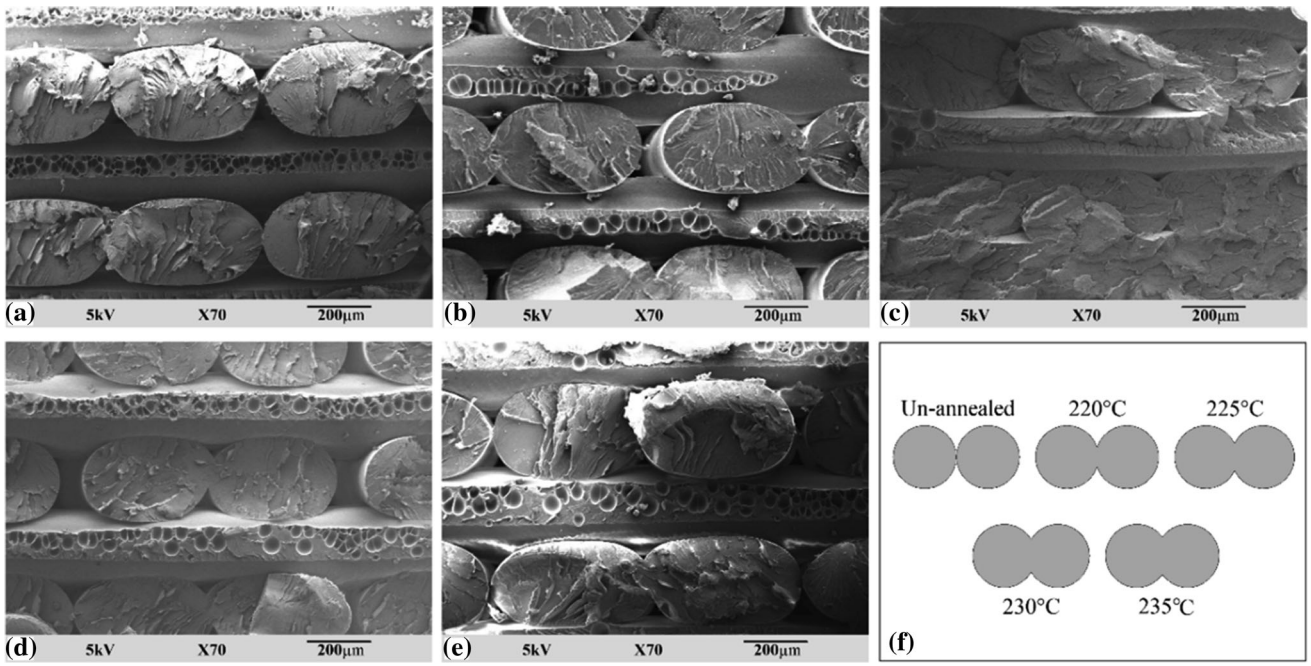

Fig. 5 SEM image of 3D printed PEI specimen: (a) unannealed, (b) annealed at 220 °C, (c) annealed at 225 °C, (d) annealed at 230 °C, (e) annealed at 235 °C, and (f) schematic representation of the change in bond formation between filaments with the annealing process

The same fracture mechanism was observed in all annealed and unannealed samples. While fiber breakage was observed in the longitudinal direction fibers, interfacial bond failure was observed in the transverse direction fibers. Fig. 5(f) illustrates that as annealing temperatures increase, the filaments' converge and the interfacial bond area increases. This indicates that the interfacial bond becomes stronger. Therefore, the lowest and highest interfacial bond area was measured in the unannealed sample and sample annealed at 235 °C, respectively (Fig. 5(a), (b), (c), (d) and (e)). As a result, it can be said that as annealing temperature increases, the interfacial bond surface area increases and the interfacial

bonds become stronger, thanks to the diffusion of PEI molecules.

3.4 Tensile Test Results

Figure 6 shows the tensile test results for unannealed and annealed 3D printed PEI specimens. The unannealed sample has a tensile strength of 68.12 MPa. It was observed that the tensile strength of the samples gradually increased with annealing temperature up to 225 °C. However, when the annealing process is applied above 225 °C, the tensile stress value of PEI material decreases slightly. The tensile strengths of all annealed samples are higher than that of the unannealed sample. The maximum increase in tensile strength was observed to be 75.11 MPa, representing an increase of approximately 10.3% in the sample annealed at 225 °C compared with the unannealed sample. This increase in strength can be explained by the formation of higher interlayer diffusion of PEI molecules during the annealing process.

The SEM images (Fig. 5) show that the bonding zone between the interfaces increases with increasing annealing temperature; therefore, strength is expected to increase as the annealing temperature is increased. However, while increasing the annealing temperature has a favorable effect in terms of bonding surface area, it also has detrimental effects in terms of thermal distortion.

The annealing operation is considered to improve the crystallinity of the polymer by reconstructing the chains in the amorphous region (Ref 53, 54). Higher crystallinity tended to provide a suitable tensile strength, but an annealing operation performed at high temperature could also lead to unexpected overheating problems such as thermal distortion and residual stress that reduced tensile strength (Ref 55–57). It is understood from the XRD results (Fig. 3) that the crystallinities of the samples annealed at 220 and 225 °C are different to those annealed at 230 and 235 °C. Hence, one of the reasons for the decrease in tensile stress is considered to be the crystallinity index.

It can be said that the tensile strength increases with increasing annealing temperature above the glass transition point, but thermal distortions are observed in samples where the annealing temperature is greater than 225 °C. While there is no thermal distortion in the samples annealed at 220 and 225 °C, those annealed at 230 and 235 °C have distortions due to high temperature. Fig. 7 shows images of the kind of distortion that can occur in these samples.

However, when the samples are subjected to higher annealing temperatures, they can show considerable deformation under their own weight (Ref 36). Thermal distortion of the samples during the post-process annealing of 3D printed creates residual stress and residual distortion (Ref 58). During the test, the tensile strength of the samples annealed at 230 and 235 °C decreased due to these residual stresses and residual distortions. Although the interfacial bonds of annealed samples has strengthened, it is thought that the tensile strength of specimens decreases due to these residual stresses (Ref 31, 59).

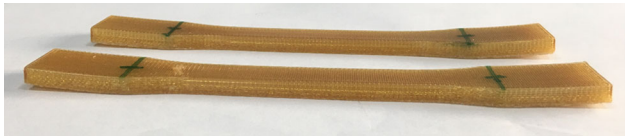

Fig. 7 Images of samples showing thermal distortion

Figure 8 shows the fracture strain of 3D printed PEI polymer specimens subjected to the annealing process. The fracture strain of the specimens was affected by annealing operations, but does not follow an increasing trend, unlike the tensile strength values. The unannealed sample has a fracture strain of 5.07, while samples annealed at 220, 225, 230, and 235 °C have fracture strains of 4.49, 4.38, 4.01 and 3.37, respectively. Tensile test results show that when the samples are heat-treated, their fracture strain decreases slightly. This behavior was likely due to the effect of the increased stiffness with increasing annealing temperature. This is consistent with a previous finding, where Harris et al. (Ref 53) reported a decrease of elongation at break with the annealing process. However, fracture strain did not significantly change within the annealed specimens. Tensile test results for samples annealed at 220, 225 and 230 °C showed higher stress levels and lower fracture strain levels, indicating brittle behavior. Annealed specimens show poor ductility and this suggests that heat treatment operations result in a loss in ductility.

3.5 Bending Test Results

Bending test results are shown in Fig. 9. The flexural strength and maximum bending force of all annealed samples are higher than that of the unannealed sample. It can be said that bending test results follow a similar trend to tensile test results. The flexural strength of the PEI specimens slightly increases up to an annealing temperature of 225 °C. However, above 225 °C, the bending strength of PEI follows a gradually decreasing trend. The maximum strength increment was seen in the sample annealed at 225 °C.

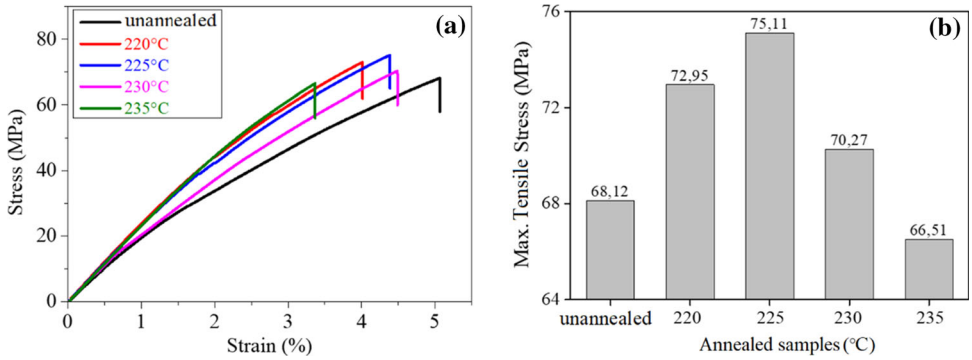

Fig. 6 Tensile test results; (a) stress–strain curve of PEI samples (b) maximum tensile stress comparison of PEI samples

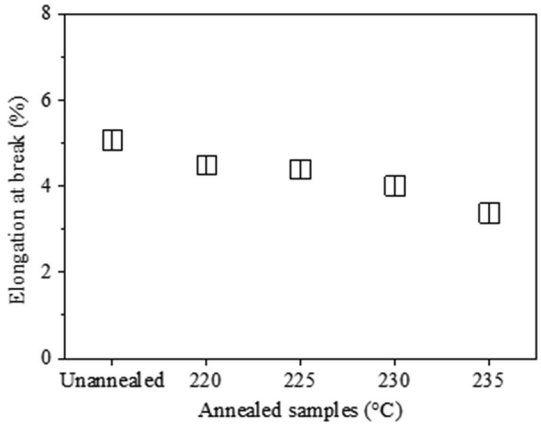

Fig. 8 Elongation at break of for 3D printed PEI polymer specimens

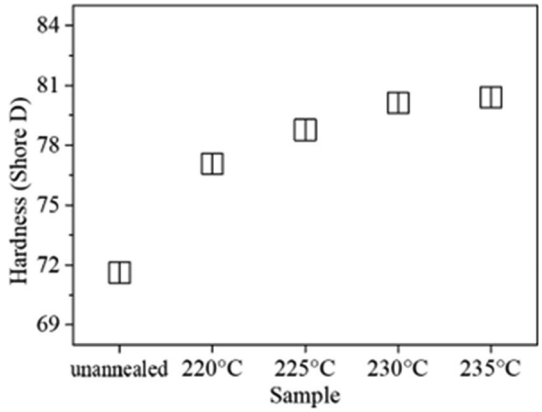

Fig. 10 Hardness test results for 3D printed PEI polymer specimens

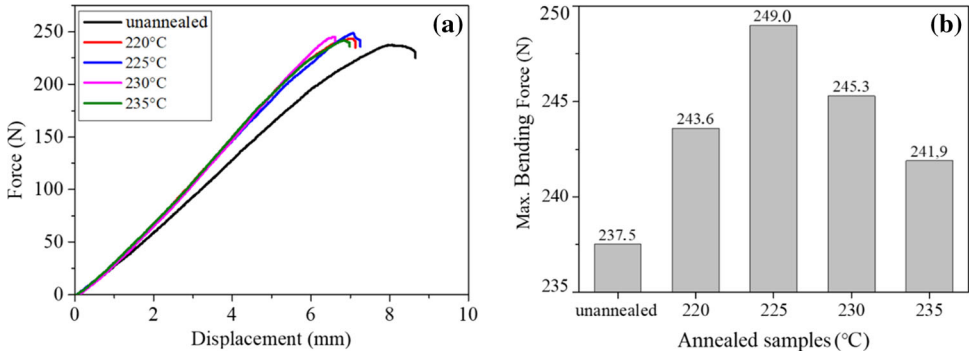

Fig. 9 Bending test results; (a) maximum force and displacement curve of PEI samples, (b) maximum force comparison of PEI samples

Heat treatment of PEI specimens above the glass transition temperature facilitates interlayer diffusion of PEI molecules, resulting in increased interlayer bonding and hence mechanical performance, as explained in a number of research studies (Ref 39–43). However, as the annealing temperature increases above 225 °C, thermal distortions occur in the sample. In addition, the PEI material becomes even more brittle. Therefore, the bending strength starts to decrease above 225 °C.

3.6 Hardness Test Results

D-type shore hardness test results for unannealed and annealed PEI specimens are presented in Fig. 10. The shore hardness, which is the most widely used method for plastic hardness measurement (Ref 60), is defined as the polymer material's resistance to the immersion of a rigid indenter into its surface layers and is determined from the indentation depth of the indenter in the polymer material under test. The hardness of all annealed samples increased compared to the unannealed sample. The greatest hardness was measured in the sample annealed at 235 °C, representing an increase of about 12.3%. As the annealing temperature was increased, the hardness of the PEI samples increased. However, above an annealing temperature of 225 °C, the increase in hardness with temperature levels off somewhat.

It is thought that the increase in hardness of the specimens is due to two reasons. The first is that the micro-voids within the microstructure of the 3D printed part were made smaller by the annealing operation (Ref 61). The size and magnitude of these micro-voids might vary depending on the annealing temperature of the specimens and might cause changes in the hardness of the tested sample. During the insertion of the rigid indenter, each layer beneath the surface of the specimens produced by the 3D printer via FDM is exposed to indentation force along with indentation depth. If the indenter frequently encounters micro-voids, the hardness decreases as the indenter will encounter less resistance during the hardness measurement. Another reason is that the interfacial bonds become stronger with the heat treatment process. Lack of strong bonding between the layers during the 3D printing process was most likely the reason for the low hardnesses of the printed parts. Since the annealing process improves the interfacial bonds and increases diffusion, the indenter encounters more resistance during measurement and this results in an apparent increase in hardness. In addition, the tensile test results show that the brittleness increases as a result of the decrease in the fracture strain, which is further proof of the increase in hardness.

The mechanical behavior of the printed PEI parts was determined from three successive mechanical test results. The best mechanical test results were observed in the samples annealed at 225 °C compared with the unannealed specimens. However, mechanical properties worsen in annealing processes carried out above 225 °C. In fact, the maximum tensile strength of the sample annealed at 235 °C was found to be 66.51 MPa, which is lower when compared to an unannealed sample. Contrary to the tension and bending test results, hardness increases with increasing temperature.

Table 2 Summary of post-processing methods used to enhance the mechanical performance of 3D printed parts as provided in the literature

Reference	3D printed material	Post-processing method	Mechanical performance of 3D printed parts
(Ref 62)	ABS	Ultrasound process at 20 kHz	10.8% improvement in flexural strength was observed
(Ref 63)	CF-reinforced ABS	Annealing at 65 °C for 60 minutes	Tensile strength increased by 16.8%
	CF-reinforced PLA	Annealing at 110 °C for 60 minutes	Tensile strength increased by 3.34%
	CF-reinforced PETG	Annealing at 85 °C for 60 minutes	Tensile strength increased by 12.4%
(Ref 64)	Cu-reinforced PLA	Laser treatment via 200 W fiber laser	Tensile strength improved by 25.6% and Young's modulus improved by 34.1%.
(Ref 65)	PLA	Annealing at 85 °C and 95 °C for 70 minutes and 15 minutes, respectively	Flexural strength improved by 17% and 11% via annealing at 85 and 95 °C.
(Ref 66)	PLA	Laser treatment vi 2.84 W diode laser	Tensile strength improved by approximately 10%.
(Ref 67)	ULTEM 9085	Annealing at 200 °C for 180 minutes	Flexural strength improved by 20%
This work	PEI/ULTEM 1010	Annealing at 220 °C, 225 °C, 230 °C, and 235 °C for 180 minutes	Tensile strength improved by 10% annealed at 225 °C.
			Flexural strength improved by 5% annealed at 225 °C.
			Hardness improved by 12% annealed at 235 °C.

The mechanical performance of the annealed parts was compared with the FDM printed parts reported in the literature and is tabulated in Table 2. When comparing the approaches in Table 2 with the annealing process, it becomes clear that annealing is a suitable post-processing procedure for enhancing interlayer mechanical performances. Ultrasonic strengthening is usually carried out on simple shape 3D printed parts intended for short-term use (Ref 62). The need for new molds for each product printed with 3D printers would make the ultrasonic strengthening system unsuitable for complex 3D printed parts. As the laser only irradiates the outer surface of the 3D printed part during the laser treatment process (Ref 64, 66), the surface and near subsurface layers of the specimen are strengthened. The annealing process does not involve any changes to the 3D printing process, and it can be used to improve the mechanical performance of the 3D printed parts.

4. Conclusions

The change in properties of polyetherimide (PEI/ULTEM 1010) material, which is preferred because of its high strength compared to conventional 3D printer materials, due to annealing was investigated in order to gain a better understanding of the interlayer adhesion strength response and thus overcome a mechanical performance limitation of this material. 225 °C was determined to be the most effective temperature for post-process annealing of the 3D printed PEI polymer. In the case of annealing at temperatures higher than 225 °C, some detrimental behavior, such as thermal degradation, is observed. The annealing process solved the problems of crystallinity reduction induced by the rapid cooling during the 3D part production and poor interfacial bond formation. Therefore, it can be said that the interlayer mechanical properties of the 3D printed PEI polymer are improved. Lower tensile stresses and bending forces were observed at higher annealing temperatures. It is observed that, according to the tensile test results, the maximum tensile stress in the annealed sample at 235 °C was lower than that in the unannealed sample. The hardness test results showed that the hardness of the material increased as the annealing temperature increased. These results confirmed that PEI materials, which were kept slightly above the glass transition temperature and cooled slowly in the oven, increased the strength of their interlayer adhesion by forming a more stable and crystalline structure. Therefore, this study demonstrates the efficiency of using the post-processing annealing process of 3D printed PEI polymer and contributes to a scientific understanding of crystallinity and mechanical property change when subjected to heat treatment. These results are extremely useful with regard to improvements in PEI material, which is a high-performance FDM thermoplastic that offers excellent strength, and thermal stability, and whose use is thus often preferred in industry for application.

Acknowledgment

This work was supported by the Scientific Research Projects Unit (BAPYB) of Gaziantep University (Project numbers: RM.16.01). The authors would like to thank the Ulug Bey High Technology Application and Research Centre (ULUTEM) in Gaziantep University.

Author Contributions

MY contributed to conception and design of study, investigation, and writing–original draft preparation. NFY contributed to methodology, project administration, and reviewing and editing. MFK contributed to investigation and design of study.

References

1. R. Singh and J.P. Davim, Additive Manufacturing: Applications and Innovations. (CRC Press, 2018.)
2. T. Pereira, J.V. Kennedy and J. Potgieter, A Comparison of Traditional Manufacturing vs Additive Manufacturing, the Best Method for the Job, *Procedia Manuf.*, 2019, **30**, p 11–18
3. J.P. Davim, "Additive and Subtractive Manufacturing: Emergent Technologies. (Walter de Gruyter GmbH, Co KG, 2020)
4. K.S. Prakash, T. Nancharaih and V.V.S. Rao, Additive Manufacturing Techniques in Manufacturing-an Overview, *Mater. Today Proc.*, 2018, **5**(2), p 3873–3882
5. J. Pou, A. Riveiro, and P. Davim, "Additive Manufacturing," Elsevier, 2021
6. O. Abdulhameed, A. Al-Ahmari, W. Ameen and S.H. Mian, Additive Manufacturing: Challenges, Trends, and Applications, *Adv. Mech. Eng.*, 2019, **11**(2), p 1687814018822880
7. J. Jiang, A Novel Fabrication Strategy for Additive Manufacturing Processes, *J. Clean. Prod.*, 2020, **272**, p 122916
8. K. Das, P. Tandon and A. Singh, 3D Printing–Imaging the Future Layer by Layer, *J. Contemp. Orthod.*, 2020, **4**(3), p 44–48
9. J.Y. Wong and A.C. Pfahnl, 3D Printing of Surgical Instruments for Long-Duration Space Missions, *Aviat. Space. Environ. Med.*, 2014, **85**(7), p 758–763
10. P. Bere, C. Neamtu and R. Udroiu, Novel Method for the Manufacture of Complex CFRP Parts Using FDM-Based Molds, *Polymers (Basel).*, 2020, **12**(10), p 2220
11. L. Novakova-Marcincinova, J. Novak-Marcincin, J. Barna, and J. Torok, "Special Materials Used in FDM Rapid Prototyping Technology Application," 2012 IEEE 16th International Conference on Intelligent Engineering Systems (INES), IEEE, 2012, p 73–76
12. X. Han, D. Yang, C. Yang, S. Spintzyk, L. Scheideler, P. Li, D. Li, J. Geis-Gerstorfer and F. Rupp, Carbon Fiber Reinforced PEEK Composites Based on 3D-Printing Technology for Orthopedic and Dental Applications, *J. Clin. Med.*, 2019, **8**(2), p 240
13. R. Sharma, R. Singh, R. Penna and F. Fraternali, Investigations for Mechanical Properties of Hap, PVC and PP Based 3D Porous Structures Obtained through Biocompatible FDM Filaments, *Compos. Part B Eng.*, 2018, **132**, p 237–243
14. Y. Zhao, K. Zhao, Y. Li and F. Chen, Mechanical Characterization of Biocompatible PEEK by FDM, *J. Manuf. Process.*, 2020, **56**, p 28–42
15. N.E. Zander, Recycled Polymer Feedstocks for Material Extrusion Additive Manufacturing, *Polymer-Based Additive Manufacturing: Recent Developments*. J.E. Seppala, A.P. Kotula, C.R. Snyder Ed., American Chemical Society, Washington, 2019, p 37–51. https://doi.org/10.1021/bk-2019-1315.ch003
16. K.G. Mostafa, C. Montemagno and A.J. Qureshi, Strength to Cost Ratio Analysis of FDM Nylon 12 3D Printed Parts, *Procedia Manuf.*, 2018, **26**, p 753–762
17. H. Wu, M. Sulkis, J. Driver, A. Saade-Castillo, A. Thompson and J.H. Koo, Multi-Functional ULTEM^{TM} 1010 Composite Filaments for Additive Manufacturing Using Fused Filament Fabrication (FFF), *Addit. Manuf.*, 2018, **24**, p 298–306
18. A. Slonov, I. Musov, A. Zhansitov, E. Rzhevskaya, D. Khakulova and S. Khashirova, The Effect of Modification on the Properties of Polyetherimide and Its Carbon-Filled Composite, *Polymers (Basel).*, 2020, **12**(5), p 1056
19. G. Taylor, X. Wang, L. Mason, M.C. Leu, K. Chandrashekhara, T. Schniepp, and R. Jones, (2018). Flexural Behavior of Additively Manufactured Ultem 1010: Experiment and Simulation. Rapid Prototyp. J
20. M. Fischer and V. Schöppner, Fatigue Behavior of FDM Parts Manufactured with Ultem 9085, *Jom*, 2017, **69**(3), p 563–568
21. G. Taylor, S. Anandan, D. Murphy, M. Leu and K. Chandrashekhara, Fracture Toughness of Additively Manufactured ULTEM 1010, *Virtual Phys. Prototyp.*, 2019, **14**(3), p 277–283
22. U.K. Komal, B.K. Kasaudhan and I. Singh, Comparative Performance Analysis of Polylactic Acid Parts Fabricated by 3D Printing and Injection Molding, *J. Mater. Eng. Perform.*, 2021, **30**(9), p 6522–6528
23. O.A. Mohamed, S.H. Masood and J.L. Bhowmik, Experimental Investigation of Time-Dependent Mechanical Properties of PC-ABS Prototypes Processed by FDM Additive Manufacturing Process, *Mater. Lett.*, 2017, **193**, p 58–62
24. M. Manjaiah, K. Raghavendra, N. Balashanmugam, and J.P. Davim, "Additive Manufacturing: A Tool for Industrial Revolution 4.0," Elsevier, 2021
25. S.R. Rajpurohit and H.K. Dave, (2018) Effect of Process Parameters on Tensile Strength of FDM Printed PLA Part. Rapid Prototyp. J. Emerald Publishing Limited
26. R. Kotsilkova, I. Petrova-Doycheva, D. Menseidov, E. Ivanov, A. Paddubskaya and P. Kuzhir, Exploring Thermal Annealing and Graphene-Carbon Nanotube Additives to Enhance Crystallinity, Thermal, Electrical and Tensile Properties of Aged Poly (Lactic) Acid-Based Filament for 3D Printing, *Compos. Sci. Technol.*, 2019, **181**, p 107712
27. D. Jiang and D.E. Smith, Anisotropic Mechanical Properties of Oriented Carbon Fiber Filled Polymer Composites Produced with Fused Filament Fabrication, *Addit. Manuf.*, 2017, **18**, p 84–94
28. B. Akhoundi, M. Nabipour, F. Hajami and D. Shakoori, An Experimental Study of Nozzle Temperature and Heat Treatment (Annealing) Effects on Mechanical Properties of High-Temperature Polylactic Acid in Fused Deposition Modeling, *Polym. Eng. Sci.*, 2020, **60**(5), p 979–987
29. J. Butt and R. Bhaskar, Investigating the Effects of Annealing on the Mechanical Properties of FFF-Printed Thermoplastics, *J. Manuf. Mater. Process.*, 2020, **4**(2), p 38
30. C. Benwood, A. Anstey, J. Andrzejewski, M. Misra and A.K. Mohanty, Improving the Impact Strength and Heat Resistance of 3D Printed Models: Structure, Property, and Processing Correlationships during Fused Deposition Modeling (FDM) of Poly (Lactic Acid), *Acs Omega,* 2018, **3**(4), p 4400–4411
31. Y. Song, Y. Li, W. Song, K. Yee, K.-Y. Lee and V.L. Tagarielli, Measurements of the Mechanical Response of Unidirectional 3D-Printed PLA, *Mater. Des.*, 2017, **123**, p 154–164
32. D.C. Bassett, R.H. Olley and I. Al Raheil, On Crystallization Phenomena in PEEK, *Polymer (Guildf).*, 1988, **29**(10), p 1745–1754
33. M. Sharma, V. Sharma, and P. Kala, "Optimization of Process Variables to Improve the Mechanical Properties of FDM Structures," *Journal of Physics: Conference Series*, IOP Publishing, 2019, p 12061
34. P. Han, A. Tofangchi, A. Deshpande, S. Zhang and K. Hsu, An Approach to Improve Interface Healing in FFF-3D Printed Ultem 1010 Using Laser Pre-Deposition Heating, *Procedia Manuf.*, 2019, **34**, p 672–677
35. S. Singh, M. Singh, C. Prakash, M.K. Gupta, M. Mia and R. Singh, Optimization and Reliability Analysis to Improve Surface Quality and Mechanical Characteristics of Heat-Treated Fused Filament Fabricated Parts, *Int. J. Adv. Manuf. Technol.*, 2019, **102**(5–8), p 1521–1536
36. S. Bhandari, R.A. Lopez-Anido and D.J. Gardner, Enhancing the Interlayer Tensile Strength of 3D Printed Short Carbon Fiber Reinforced PETG and PLA Composites via Annealing, *Addit. Manuf.*, 2019, **30**, p 100922
37. I.M. Balashova, R.P. Danner, P.S. Puri and J.L. Duda, Solubility and Diffusivity of Solvents and Nonsolvents in Polysulfone and Polyetherimide, *Ind. Eng. Chem. Res.*, 2001, **40**(14), p 3058–3064
38. Stratasys, "ULTEM 1010 Resin ULTEM 1010 Resin," n.d., p 1–3, https://arti90.com/wp-content/uploads/2018/01/Spec-Sheet-ULTEM-1010-EN-A4-1.pdf
39. P.G. de Gennes, Reptation of a Polymer Chain in the Presence of Fixed Obstacles, *The J. Chem. Phys.*, 1971, **55**(2), p 572–579. https://doi.org/10.1063/1.1675789
40. Y.H. Kim and R.P. Wool, A Theory of Healing at a Polymer-Polymer Interface, *Macromolecules*, 1983, **16**(7), p 1115–1120
41. Q. Sun, G.M. Rizvi, C.T. Bellehumeur and P. Gu, Effect of Processing Conditions on the Bonding Quality of FDM Polymer Filaments, *Rapid Prototyp. J.*, 2008, **14**(2), p 72–80. https://doi.org/10.1108/13552540810862028

42. S. Prager and M. Tirrell, The Healing Process at Polymer-Polymer Interfaces, *J. Chem. Phys.*, 1981, **75**(10), p 5194–5198
43. T. Ge, M.O. Robbins, D. Perahia and G.S. Grest, Healing of Polymer Interfaces: Interfacial Dynamics, Entanglements, and Strength, *Phys. Rev. E*, 2014 https://doi.org/10.1103/PhysRevE.90.012602
44. A. D638-14, ASTM International, *Stand. test method tensile Prop. Plast.*, 2014
45. A. International, ASTM D790−17-Flexural Properties of Unreinforced and Reinforced Plastics and Electrical Insulating Materials, 2017
46. A. Standard, D2240-15 Standard Test Method for Rubber Property–Durometer Hardness, 2015
47. B.-K. Chen, C.-T. Su, M.-C. Tseng and S.-Y. Tsay, Preparation of Polyetherimide Nanocomposites with Improved Thermal Mechanical and Dielectric Properties, *Polym. Bull.*, 2006, **57**(5), p 671–681
48. A. Choudhury, Dielectric and Piezoelectric Properties of Polyetherimide/BaTiO3 Nanocomposites, *Mater. Chem. Phys.*, 2010, **121**(1–2), p 280–285
49. R.N. Muthu, S. Rajashabala, and R. Kannan, Synthesis of Polyetherimide/Halloysite Nanotubes (PEI/HNTs) Based Nanocomposite Membrane towards Hydrogen Storage, *AIP Conference Proceedings*, (AIP Publishing LLC, 2018) p 50107
50. M. Owlad, M.K. Aroua and W.M.A.W. Daud, Hexavalent Chromium Adsorption on Impregnated Palm Shell Activated Carbon with Polyethyleneimine, *Bioresour. Technol.*, 2010, **101**(14), p 5098–5103
51. A. D5573-99, (2012) Standard Practice for Classifying Failure Modes in Fiber-Reinforced-Plastic (FRP) Joints. Annual Book of ASTM Standards. p 2002
52. N. Wang and S. Xia, Cohesive Fracture of Elastically Heterogeneous Materials: An Integrative Modeling and Experimental Study, *J. Mech. Phys. Solids.*, 2017, **98**, p 87–105
53. A.M. Harris and E.C. Lee, Improving Mechanical Performance of Injection Molded PLA by Controlling Crystallinity, *J. Appl. Polym. Sci.*, 2008, **107**(4), p 2246–2255
54. M. Zhu, J. Han, F. Wang, W. Shao, R. Xiong, Q. Zhang, H. Pan, Y. Yang, S.K. Samal and F. Zhang, Electrospun Nanofibers Membranes for Effective Air Filtration, *Macromol. Mater. Eng.*, 2017, **302**(1), p 1600353
55. M. Hesami and A. Jalali-Arani, Cold Crystallization Behavior of Poly (Lactic Acid) in Its Blend with Acrylic Rubber; the Effect of Acrylic Rubber Content, *Polym. Int.*, 2017, **66**(11), p 1564–1571
56. C. Yang, X. Tian, D. Li, Y. Cao, F. Zhao and C. Shi, Influence of Thermal Processing Conditions in 3D Printing on the Crystallinity and Mechanical Properties of PEEK Material, *J. Mater. Process. Technol.*, 2017, **248**, p 1–7
57. B.S. Thakkar and L.J. Broutman, Impact Strength of Polymers. 3: The Effect of Annealing on Cold Worked Polycarbonates, *Polym. Eng. Sci.*, 1981, **21**(3), p 155–162. https://doi.org/10.1002/pen.760210308
58. J. Cao, M.A. Gharghouri, and P. Nash, Finite-Element Analysis and Experimental Validation of Thermal Residual Stress and Distortion in Electron Beam Additive Manufactured Ti-6Al-4V Build Plates, *J. Mater. Process. Technol.*, Elsevier, 2016, **237**, p 409–419
59. A.A. D'Amico, A. Debaie, and A.M. Peterson, (2017) Effect of Layer Thickness on Irreversible Thermal Expansion and Interlayer Strength in Fused Deposition Modeling, Rapid Prototyp. J. Emerald Publishing Limited
60. A. Štibler, K. Herrmann, and Z. Šušteri, "Long-Term Stability of Rubber Hardness Reference Blocks," HARDMEKO, 2004
61. G. Liao, Z. Li, C. Luan, Z. Wang, X. Yao and J. Fu, Additive Manufacturing of Polyamide 66: Effect of Process Parameters on Crystallinity and Mechanical Properties, *J. Mater. Eng. Perform.*, 2022, **31**(1), p 191–200
62. W. Wu, J. Jiang, H. Jiang, W. Liu, G. Li, B. Wang, M. Tang and J. Zhao, Improving Bending and Dynamic Mechanics Performance of 3D Printing through Ultrasonic Strengthening, *Mater. Lett.*, 2018, **220**, p 317–320
63. S. Rangisetty and L.D. Peel, "The Effect of Infill Patterns and Annealing on Mechanical Properties of Additively Manufactured Thermoplastic Composites," *Smart Materials, Adaptive Structures and Intelligent Systems*, (American Society of Mechanical Engineers, 2017) p V001T08A017
64. L. Chen, X. Zhang, Y. Wang and T.A. Osswald, Laser Polishing of Cu/PLA Composite Parts Fabricated by Fused Deposition Modeling: Analysis of Surface Finish and Mechanical Properties, *Polym. Compos.*, 2020, **41**(4), p 1356–1368
65. R.A. Wach, P. Wolszczak and A. Adamus-Wlodarczyk, Enhancement of Mechanical Properties of FDM-PLA Parts via Thermal Annealing, *Macromol. Mater. Eng.*, 2018, **303**(9), p 1800169
66. N. Sabyrov, A. Abilgaziyev and M. Ali, Enhancing Interlayer Bonding Strength of FDM 3D Printing Technology by Diode Laser-Assisted System, *Int. J. Adv. Manuf. Technol.*, 2020, **108**(1), p 603–611
67. A.C. de Bruijn, G. Gómez-Gras and M.A. Pérez, Thermal Annealing as a Post-Process for Additively Manufactured Ultem 9085 Parts, *Procedia Comput. Sci.*, 2022, **200**, p 1308–1317